

AS-TEXONO/01-04

February 19, 2019

Nuclear Recoil Measurement in CsI(Tl) Crystal for Cold Dark Matter Detection

M.Z. Wang^a, Q. Yue^b, J.R. Deng^c, W.P. Lai^{d,e}, H.B. Li^{a,d}, J. Li^b,
Y. Liu^b, B.J. Qi^c, X.C. Ruan^c, C.H. Tang^a, H.Q. Tang^c,
H.T. Wong^{d,*}, S.C. Wu^a, B. Xin^c, Z.Y. Zhou^c

^aDepartment of Physics, National Taiwan University, Taipei, Taiwan.

^bInstitute of High Energy Physics, Beijing, China.

^cDepartment of Nuclear Physics, Institute of Atomic Energy, Beijing, China

^dInstitute of Physics, Academia Sinica, Taipei, Taiwan.

^eDepartment of Management Information Systems, Chung Kuo Institute of Technology,
Taipei, Taiwan.

*Corresponding author: Email: htwong@phys.sinica.edu.tw; Tel:+886-2-2789-9682; FAX:+886-2-2788-9828.

Abstract

There are recent interests with CsI(Tl) scintillating crystals for Dark Matter experiments. The scattering signatures by neutrons on a CsI(Tl) detector were studied using a neutron beam generated by a 13 MV Tandem accelerator. The energy spectra of nuclear recoils from 7 keV to 132 keV were measured, and their quenching factors for scintillating light yield were derived. The data confirms the Optical Model predictions on neutron elastic scatterings with a direct measurement of the nuclear recoils on heavy nuclei. The pulse shape discrimination techniques to differentiate nuclear recoils from γ -background were studied. Internal consistencies were obtained among the different methods of light yield measurements. The projected capabilities for Cold Dark Matter searches with CsI(Tl) crystals are presented.

PACS Codes: 25.40.Dn, 95.35.+d, 29.40.Mc.

Keywords: Neutron elastic scattering, Dark matter, Scintillation detectors.

1 Introduction

The detection of Dark Matter and the studies of their properties [1] are of fundamental importance in particle physics and cosmology. The Weakly Interacting Massive Particles (WIMPs) are good candidates for “Cold” Dark Matter, and their experimental searches have gathered a lot of interests in recent years. The most promising avenue is to detect the nuclear recoil signatures due to elastic scatterings of WIMPs on the target isotopes. The typical energy depositions are only of the order of 10 keV, imposing big experimental challenges in terms of the detection of weak signals as well as background control at low energy close to detection threshold. A wide spectrum of experimental techniques is being pursued [2].

The DAMA experiment observed an annual modulation of nuclear recoil events [3] with NaI(Tl) scintillating crystal detectors, which can be interpreted as positive evidence of WIMPs due to the difference of the relative velocities of the Earth from the Halo sea within the year. This, however, contradicts the limit from the CDMS experiment [4] based on cryogenic technique.

There is still much room for new detector concept to thoroughly test the DAMA parameter space, and to push the sensitivities further. It would be of great interest if the sensitivities of WIMP searches can probe the level predicted by the various Super-Symmetry models.

There are potential merits of using CsI(Tl) scintillating crystals [5] for WIMP search and other low-energy low-background experiments [6, 7]. An experiment towards 200 kg of CsI(Tl) crystal scintillators to study low energy neutrino interactions at the Kuo-Sheng power reactor is being pursued [7], while the adaptation of the crystal for Dark Matter searches are the focus of several on-going projects [8, 9, 10, 11].

The high-A content of the CsI enhances the sensitivities for the spin-independent interactions (which depends on A^2) between the WIMPs and the target, relative to most other candidate target isotopes. The high-Z composition allows a compact design and provides large suppression of background due to ambient radioactivity if a three dimensional fiducial volume definition can be realized. Both ^{133}Cs and ^{127}I are 100% in their respective isotopic abundance. Being close in their mass numbers, the response to nuclear recoil from the interactions with WIMPs would be similar, allowing simpler interpretation of experimental signatures.

As a detector, the crystal has large light yield, low energy threshold and with pulse shape discrimination characteristics for γ/α separation. Its characteristics of being only slightly hygroscopic implies that it can be machined easily and does not require hermetic

seal (that is, passive materials) in a large detector system. In addition, large (40 tons) electromagnetic calorimeter systems [12] have been constructed and made operational in high energy physics experiments, making this technology affordable and realistic to scale up. Considering all the associated costs, the price of CsI(Tl) is in fact less than that for NaI(Tl). In order to produce positive and definite evidence of the WIMPs, an accurate measurement of the annual modulation (where the maximal effects are only 7%) would be necessary such that the availability of large target mass is a very desirable feature.

One of the key issues to realize a Dark Matter search experiment with CsI(Tl) crystal scintillator is the studies of the experimental signatures of nuclear recoils due to WIMP-nuclei elastic scatterings. Nuclear recoils produce large charge density (dE/dx) such that the scintillating light yield is “quenched” and the timing profile of pulse shape is different relative to the same energy deposition by minimum ionizing particles [13].

These signatures are the same as the nuclear recoil events produced by elastic scattering of neutrons on nuclei. A measurement was performed with the neutron facility at the 13 MV Tandem accelerator at the China Institute of Atomic Energy at Beijing. The results of the quenching factors measurement and of pulse shape discrimination studies are reported in this article. There are other recent measurements work on CsI(Tl) [8, 9], as well as on other scintillating crystals such as NaI(Tl) and $\text{CaF}_2(\text{Eu})$ [14].

2 Experimental Setup and Procedures

The experiment was performed at HI-13 tandem accelerator at the China Institute of Atomic Energy (CIAE) in Beijing. A schematic diagram is shown in Figure 1. A pulsed deuteron beam at 5.6 MeV interacted with a deuterium gas target in a cell at a pressure of 6 bar and the dimensions of 1 cm in diameter and 3 cm in length. Neutrons at 8 MeV kinetic energy were produced at zero degree. The CsI(Tl) sample was located 2.02 meters away from the deuterium target. Neutrons at zero degree were selected by a 32 mm by 35 mm collimator of length 1.2 m. The collimator were surrounded by shielding materials like iron, paraffin, lead and polyethylene to reduce background. During this data taking, the repetition rate of the pulsed beam was set at 4 MHz and the average beam current was at 1 μA .

The scattering target, which also functioned as a detector, was a CsI(Tl) crystal scintillator[†] with diameter 3 cm and length 3 cm wrapped with teflon sheets, aluminium foil and black plastic tape. To minimize supporting structures, the detector was hung at the correct position by a piece of string. The readout was achieved by a 29 mm diameter

[†]Producer: Unique Crystal, Beijing

photo-multiplier tube (PMT)[‡] The PMT signals passed through an amplifier and shaper and were digitized by a 20 MHz, 8-bit, Flash Analog-to-Digital Converter (FADC) [15] developed for the Kuo-Sheng reactor neutrino experiment [7]. The trigger was provided from a time of flight (TOF) system to tag the elastically scattered neutrons. The γ -response of the CsI(Tl) detector was calibrated with an LED pulser operated at single photo-electron intensity, as well as standard ^{109}Cd and ^{133}Ba γ -sources. The calibration is 4 photo-electrons per keV of electron-equivalence energy.

Neutron tag was provided by liquid scintillator[§] detectors 105 mm in diameter and 50 mm in length equipped with PMT[¶] readout. The liquid scintillator provides pulse shape discrimination (PSD) capabilities for n- γ differentiation. The PSD was achieved by commercial electronics^{||}. The neutron tag signal was used to define the “START” timing for the TOF system. The pulsed deuteron “pick-off” signal provided by the accelerator was delayed and used as “STOP” for the TOF. The neutron detectors were placed at a distance of 0.5 to 2 m from the CsI(Tl) target at different angles, to provide optimized TOF resolution to differentiate events due to neutron elastic scattering off hydrogen atoms or heavier nuclei in the wrapping materials.

The FADC recorded data continuously in a circular buffer of 4k size. A START-STOP sequence from the TOF system initiated a trigger which stopped the FADC digitization after 25 μs . The pulse shape from the CsI(Tl) crystal was recorded for a pre-trigger and post-trigger periods of 5 μs and 25 μs , respectively. With the timing settings at data taking, the CsI(Tl) pulse started at $-1.25 \mu\text{s}$ if it was due to nuclear recoils of heavy nuclei. This timing information provides a powerful means of the rejection of background due to proton recoils and pile-up events.

Data taking at each scattering angle was complemented by a measurement of the TOF background spectrum with *empty* target which was made of the CsI(Tl) wrapping materials only. Displayed in Figure 2 is the TOF spectra at 50° with empty and complete target. The lower and upper peaks are due to neutron elastic scattering off protons and the heavier nuclei such as carbon, aluminium, cesium, and iodine, respectively. The flat background is due to random coincidence. It can be seen that with the CsI(Tl) target in place, the upper TOF peak for neutron scattering off heavier nuclei becomes enhanced. The difference between the two TOF spectra is the nuclear recoils spectra from Cs and I. The proton-recoil events tagged by the low TOF peak provides a means to evaluate the signal yield and to confirm the distance between neutron detector and CsI target.

[‡]CR110, Hamamatsu Photonics, China

[§]Co-261, ST-451

[¶]Philips XP-2041

^{||}CANBERRA 2160A

The reconstructed energy is defined as the pedestal-subtracted integrated area of the FADC pulse over $2.5 \mu\text{s}$ starting from the t_0 of FADC ($1.25 \mu\text{s}$ before TOF trigger in this data taking). This restricted time window helps to minimize the pile up effect from accidental low energy γ 's which are abundant along the beam line. Events are categorized into two groups by the central value between the two TOF peaks and their corresponding nuclear recoil energy spectra are compared. The energy spectra at 50° are shown in Figure 3a and 3b for events with high TOF values and low TOF values, respectively.

The energy spectrum tagged by the low TOF trigger is displayed in Figure 3b. Since the trigger is due to proton recoils from the wrapping materials, there should be no correlated signals from the CsI(Tl) target. The energy spectrum which shows a distinguished peak with long tail on the high-energy side is due to events from accidental γ 's arriving within the integration time-window.

The detector response for CsI nuclear recoil events was obtained by subtracting Figure 3b from Figure 3a with proper normalizations, where the factors are derived by normalizing the low TOF peaks from proton recoils between the full and empty target spectra.

3 Measurement Results

The resulting CsI recoil spectra obtained by the “statistical background subtraction” scheme discussed in Section 2 are shown in Figure 4 for eight different scattering angles. It can be seen that this procedure is valid since the background levels away from the peaks after subtraction are consistent with zero.

The nuclear recoil energy (T) is related to the neutron scattering angle (θ) by a simple kinematical formula:

$$T = \frac{2A}{(1+A)^2} (1 - \cos\theta) E_n \quad , \quad (1)$$

where A is the target atomic mass and E_n is the incident neutron energy. The neutron scattering angle can be considered to be the same in this case in both the laboratory and center-of-mass systems. Comparisons of the nuclear recoil spectra with those due to calibration sources allow the evaluation of the quenching factors, defined as the light yield from nuclear recoils versus that from γ sources.

To enhance the signal-to-noise ratio in the large background environment, the nuclear recoil pulses are integrated for a restricted $2.5 \mu\text{s}$ (or 50 FADC time bins), as compared to the full time window $12.5 \mu\text{s}$ (or 250 FADC time bins) for 100% light collection in the γ -sources calibration measurements. A correction factor of 1.15 is applied to the nuclear recoils light yield to account for this partial summation. This factor was derived

by averaging and comparing a large number of events due to nuclear recoils and ^{109}Cd γ -source, as depicted in Figure 5. The estimated uncertainty is 10%, based on studies with different integration time window from 1.5 μs to 12.5 μs .

The deviation from the central value of nuclear recoil energy due to finite detector size is at most 2% for different scattering angles. This is checked by calculating the average recoil energy with proper weights of event angular distribution and detector acceptance. A shift of detector at 1 mm scale has negligible effect on the central value of nuclear recoil energy. The beam current was stable at the 1% level during data taking, as indicated by the stable data taking rate (typical value is about 4 Hz) as well as readings from beam monitor counters. The main systematic uncertainties originate from the analysis procedures, and amount to 16% at the lowest energy point at 20° . The statistical and systematic uncertainties are then combined in quadrature to provide the total uncertainties for each data point.

The results at different scattering angles are summarized in Table 1. The measured quenching factors are depicted in Figure 6a, while the variation of electron-equivalence light yield (the “visible” energy) versus recoil energies are shown in Figure 6b. The other measurements [8, 9] are overlaid for comparison. There is a clear trend of less quenching towards low energy points. This measurement achieved a lower threshold and with improved uncertainty compared to Ref. [9]. The quenching factors are of the similar range to those for NaI(Tl) [16], which are typically 25% for Na and 8% for I. It can be seen that the light yield is higher for interactions with the high-A isotopes in CsI(Tl), providing big advantages to probing the spin-independent interactions. In addition, Figure 6b depicts a linear relationship between the electron-equivalence light yield and the nuclear recoil energy, as indicated by a linear fit our data set. Data from Ref. [8] shows more quenching and deviates from the linear regime at high energy. This is different from the highly non-linear response due to threshold effects observed in liquid scintillator [17] at the same range of recoil energy.

The total number of observed signal events are given by the area under the Gaussian fits in Figure 4. To derive the differential cross sections, the data taking time, the acceptance (proportional to r^{-2}) and the efficiency correction factors have to be evaluated. The efficiency factors are due to the TOF selection criteria and background subtraction scheme. The efficiency is close to 100% for the well-separated TOF peaks, but is only 42% for the worst cases where the TOF peaks overlap. The contributions from inelastic scattering leading to the low excited levels for ^{133}Cs and ^{127}I are expected to be less than 0.1% relative to the elastic processes.

After all the correction factors are taken into account, the measured angular distri-

bution for neutron elastic scatterings off Cs and I is displayed in Figure 7. The shape of the solid curve is the evaluated neutron elastic scattering cross sections on ^{133}Cs and ^{127}I from ENDF/B-VI library [18] which comes from the Optical Model calculation. The absolute normalization is from a best-fit value. There is excellent agreement between the relative recoil angular distribution from this measurement and the predictions from the Optical Model. In particular, this is a kinematical regime where the size of the nuclei is comparable to the wavelength of the incident neutrons, and the diffraction pattern is well-reproduced by the data.

The measurements demonstrate the validity of the nuclear recoil event selection procedures at all angles. In addition, the results in Figure 7 confirms the Optical Model predictions on neutron elastic scatterings from a direct measurement of nuclear recoils on heavy nuclei (instead of from the scattered final-state neutrons in transmission-type experiments) – that is, they show that neutrons do elastically scatter off from the nuclei but not via some anomalous processes.

4 Pulse Shape Discrimination

The nuclear recoil measurements provide in addition an excellent data set for the study of PSD at small photo-electron level near detection threshold. The measured nuclear recoil and γ pulse shapes, averaged over many events, are shown in Figure 5 for neutrons scattering at 50° and the 22.1 keV line from ^{109}Cd , respectively. The neutron induced nuclear recoil pulse shape is similar to that of the α source data [19] taken at high energy. It can be seen that heavily-ionizing events such as those due to α -particles and nuclear recoils have *faster* decays than those from γ 's – opposite to the response in liquid scintillator [13].

Two independent approaches to obtain PSD were studied: (1) neural network technique [20] and (2) mean-time plus partial charge method. For the neural network approach, we used 4000 events each from the above two data sets as training samples and additional 4000 events each as testing samples. The trained neural net has 20 input nodes in $5 \mu\text{s}$ window with 10 hidden nodes. The input node value should be greater than zero after pedestal correction. A negative value is reset to zero and the sum of the 20 input values are normalized to one. The algorithm used is back propagation. The excellent separation power from neural net study is depicted in Figure 8. The trained neural net is applied to the complete 50° data set. Good separation is obtained between the 43 keV nuclear recoils and the low energy γ pulses. A cut on neural output greater than 0.9 selects almost all the CsI nuclear recoil events. The number of events as well as the mean and

RMS electron-equivalence energy are consistent with those determined from the statistical background subtraction method in Section 3. The PSD separation of the 20° data set, however, is not satisfactory. The neutron-beam environment gave rise to large accidental background (mostly low energy γ -events) which produce much stronger bias for the low energy nuclear recoil signatures. This would not be a problem in a realistic Dark Matter experiment where the background rate would be extremely low.

A large simulated sample was generated at different photon-statistics situation with these recoil/ γ pulse shapes, and the results are displayed in Figure 9. It can be seen that a 95% γ rejection with >90% efficiency for pulses with an average 20 photo-electrons can be achieved. It is projected that the performance can be further improved in a low-background quiet environment which allows a longer sampling window. These are better than the PSD capabilities for NaI(Tl) detectors at the same light yield [9].

The alternative and complementary approach is the partial charge method. Two variables, the mean time $\langle t \rangle$ and the partial charge ratio R, are defined for each pulse, such that

$$\langle t \rangle = \frac{\sum_{i=1}^{50} (A_i t_i)}{\sum_{i=1}^{50} A_i} \quad (2)$$

and

$$R = \frac{\sum_{i=1}^{30} A_i}{\sum_{i=1}^{50} A_i} \quad , \quad (3)$$

where A_i is the FADC amplitude at time bin t_i . The scattered plots for $\langle t \rangle$ versus TOF as well as $\langle t \rangle$ versus R for the data set at 95° are shown in Figures 10a&b, respectively. The electron-equivalence energy for CsI recoils is 13.4 keV at this scattering angle. There are clear separations between the Cs and I nuclear recoil events, represented by the box region, and the accidental γ -background for events triggered by the recoils of the wrapping materials (protons as well as other heavy nuclei). The events due to the 22 keV γ -rays from a ^{109}Cd source are displayed in Figure 10c, indicating excellent separation between nuclear recoils from the “in-time” γ -background as well. The cuts in $\langle t \rangle$ versus R space as defined in Figure 10b are subsequently applied to the other data set at lower recoil energies to select nuclear recoil events.

The electron-equivalence light yield at different scattering angles for the nuclear recoil events selected by either of the two PSD algorithms are measured. The comparison between the two PSD algorithms with the subtraction method discussed in Section 3 is depicted in Figure 11, indicating that consistent results are obtained. The deviations

of the mean values among these independent measurements are also consistent with the estimated systematic uncertainties.

Therefore, the robustness of the quenching factor results in Figures 6a&b measured by the statistical subtraction method discussed in Section 3 is further established. This method involves a straight-forward normalization and subtraction scheme, and is therefore expected to be more unbiased compared to the two PSD algorithms.

5 Discussion and Summary

In this article, we presented a new measurement on the quenching factors of Cs and I in a CsI(Tl) crystal scintillator based on statistical background subtraction. Lower threshold and improved accuracies are achieved compared to previous measurements. The measured differential cross-section of neutron scattering from I and Cs is in excellent agreement with Optical Model derivations, and represents the first confirmation of the Optical Model on neutron elastic scattering cross-sections with a direct measurement of nuclear recoils from heavy nuclei. The recoil differential cross sections and the quenching factors are relevant to the studies of radiation damage in materials. Two complementary pulse shaping discrimination techniques at the low photo-statistics regime were studied based on the nuclear recoil data. The electron-equivalence light yield derived from these methods are consistent with those obtained by statistical subtraction. The internal consistencies of the light yield measurements among the three different algorithms and also with the Optical Model predictions of differential cross section enhance the reliability and robustness of the results.

By optimizing the detector geometry and using green-extended photo-cathode, a detector with several kg modular mass and a light yield of a few photo-electron per keV can be realized [10, 11]. The background from ambient radioactivity or intrinsic radio-purity is of course crucial to all low-background experiments. Their considerations for CsI(Tl) detectors are discussed in Refs. [6, 7, 21]. Levels of better than the 10^{-12} g/g level in concentration for the ^{238}U and ^{232}Th series have been demonstrated, assuming secular equilibrium. The potential problem of the internal ^{137}Cs contaminations can be overcome via selection of clear ore materials and careful chemical processing and purification treatment [10].

Displayed in Figure 12 is the sensitivity plot for spin-independent WIMP interaction cross section per nucleon with a target mass of 1 ton of CsI(Tl). The plot is based on the assumptions that the detection threshold is at 2 keV (or about 16 keV recoil energy) and still allows enough photo-electron statistics for background rejection with

PSD, and that the observed background rate after the PSD cuts are applied is at the same as or ten times better level than the NaI(Tl) experiments (1 and 0.1 per day per kg per keV, respectively). It can be seen that the DAMA allowed region, represented by the shaded region in Figure 12, can be thoroughly probed. Given that there is matured experience of scaling up the CsI(Tl) detector to multi-ton systems, there are potentials of further improvements in the sensitivities, and in the case of positive results, performing an accurate measurement of the annual modulation.

6 Acknowledgements

The authors would like to thank Drs. K.W. Ng and S.K. Kim for fruitful discussions, and are grateful to the technical staff from CIAE and IHEP for operating the accelerator. This work was supported by contracts CosPa 89-N-FA01-1-4-2 from the Ministry of Education, Taiwan, NSC 89-2112-M-001-056 and NSC 90-2112-M-001-037 from the National Science Council, Taiwan, and NSF19975050 from the National Science Foundation, China.

References

- [1] For an overview, see, for example, E. Kolb and M. Turner, *The Early Universe*, Addison-Wesley (1989).
- [2] For a recent review, see, for example, A. Morales, Nucl. Phys. B (Procs. Suppl.) **87**, 477 (2000).
- [3] R. Bernabei et al., Phys. Lett. **B 389**, 757 (1996);
R. Bernabei et al., Phys. Lett. **B 450**, 448 (1999).
- [4] R. Abusaidi et al., Nucl. Instrum. Meth. **A 444**, 345 (2000);
R. Abusaidi et al., Phys. Rev. Lett. **84** 5699 (2000).
- [5] H. Grassmann, E. Lorentz and H.G. Moser, Nucl. Instrum. Methods **228**, 323 (1985);
P. Schotanus, R. Kamermans, and P. Dorenbos, IEEE Trans. Nucl. Sci. **37**, 177 (1990).
- [6] H.T. Wong et al., hep-ex/9910002, Astropart. Phys. **14**, 141 (2000).
- [7] H.T. Wong and J. Li, Mod. Phys. Lett. **A 15**, 2011 (2000);
H.B. Li et al., TEXONO Coll., hep-ex/0001001, Nucl. Instrum. Methods **A 459**, 93 (2001).
- [8] S. Pecourt et al., Astropart. Phys. **11**, 457 (1999).
- [9] V.A. Kudryavtsev et al., Nucl. Instrum. Methods **A 456**, 272 (2001).
- [10] H.J. Kim et al., Nucl. Instrum. Methods **A 457**, 471 (2001);
H.J. Ahn et al., Technical Design Report, KIMS Coll. (2001).
- [11] Q. Yue et al., in preparation for Nucl. Instrum. Methods **A** (2001).
- [12] Y. Kubota et al., CLEO Coll., Nucl. Instrum. Methods **A 320**, 66 (1992);
E. Aker et al., Crystal Barrel Coll., Nucl. Instrum. Methods **A 321**, 69 (1992);
Letter of Intent, Belle Coll., KEK (1993);
Letter of Intent, BaBar Coll., SLAC-443 (1994).
- [13] See, for example, “Theory and Practice of Scintillation Counting”, J.B. Birks, Pergamon (1964).
- [14] D.R. Tovey et al, Phys. Lett. **B 433**, 150 (1998).

- [15] W.P. Lai et al., TEXONO Coll., hep-ex/0010021, Nucl. Instrum. Methods **A 465**, 550 (2001).
- [16] G. Gerbier et al., Astropart. Phys. **11**, 287 (1999).
- [17] D.J. Ficenec et al., Phys. Rev. **D 36**, 311 (1987).
- [18] <http://www.nndc.bnl.gov>, Evaluated Nuclear Data File (ENDF), National Nuclear Data Center, Brookhaven National Laboratory (2001).
- [19] Y. Liu et al., TEXONO Coll., hep-ex/0105006, Nucl. Instrum. Methods **A**, in press (2001).
- [20] C. Peterson, T. Rognvaldsson and L. Lonnblad, Comput. Phys. Comm. **81**, 185 (1994).
- [21] U. Kilgus, R. Kotthaus, and E. Lange, Nucl. Instrum. Methods **A 297**, 425, (1990); R. Kotthaus, Nucl. Instrum. Methods **A 329**, 433 (1993).

Angle ($^{\circ}$)	20	30	40	50	60	65	80	95
Neutron Detector Distance (cm)	228	133	100	89	60	63	70	68
Recoil Energy (keV)	7.3	16.2	28.4	43.3	60.6	70.0	100	132
Mean Light Output (FADC Unit)	168	311	495	676	912	1004	1428	1866
Electron-Equivalence Light Yield (keV)	1.25 \pm 0.20	2.26 \pm 0.27	3.57 \pm 0.57	4.86 \pm 0.49	6.53 \pm 0.65	7.18 \pm 0.72	10.2 \pm 1.0	13.4 \pm 1.3
Quenching Factor	0.17 \pm 0.027	0.14 \pm 0.017	0.13 \pm 0.020	0.11 \pm 0.011	0.11 \pm 0.011	0.10 \pm 0.010	0.10 \pm 0.010	0.10 \pm 0.010

Table 1: Measured results of the neutron elastic scatterings from CsI(Tl) detector. Errors shown are combined systematic and statistical uncertainties.

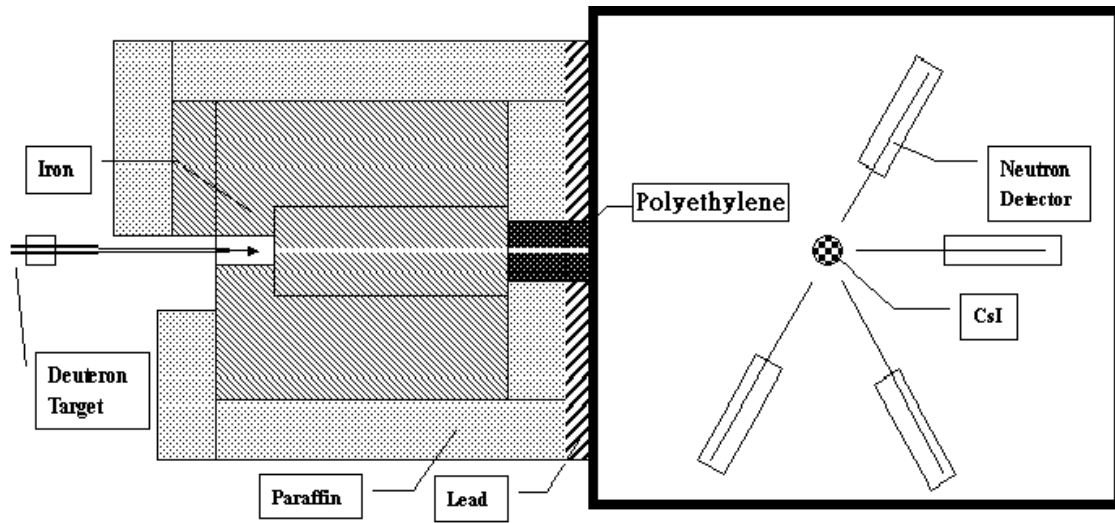


Figure 1: Schematic diagram of the experimental set-up.

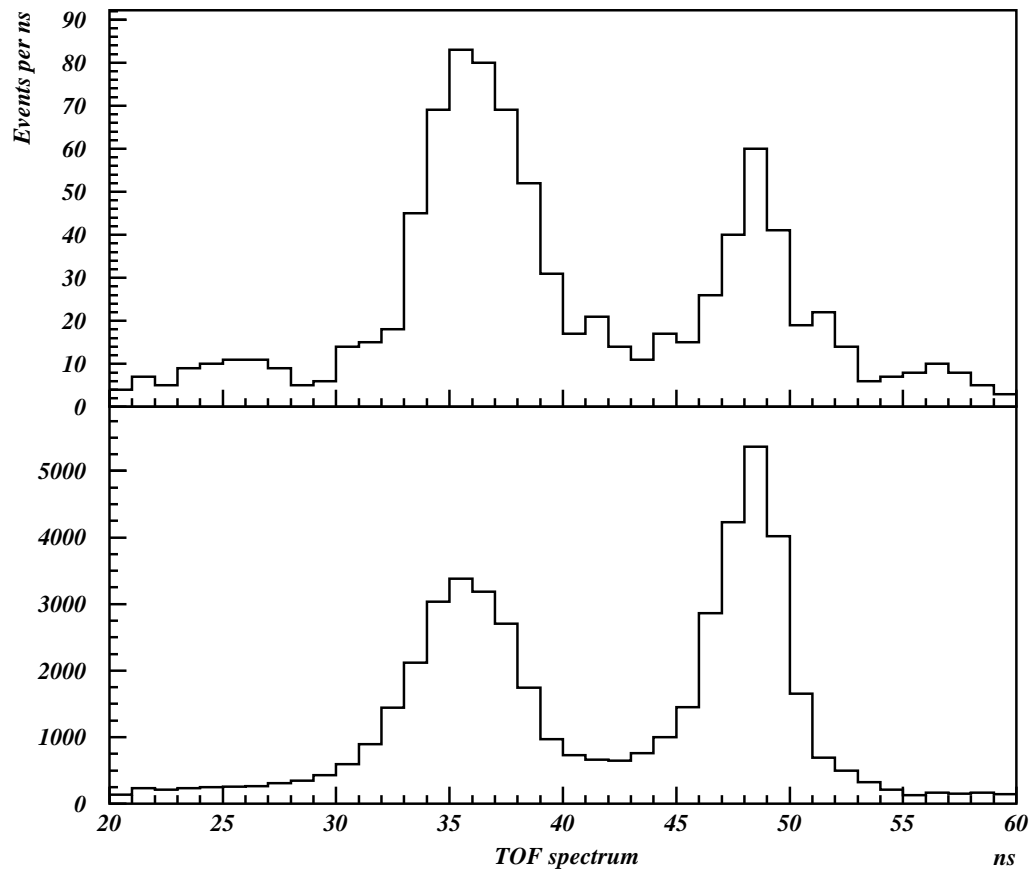


Figure 2: The TOF spectra at 50° scattering angle for (a) with wrapping material only, (b) with CsI(Tl) target.

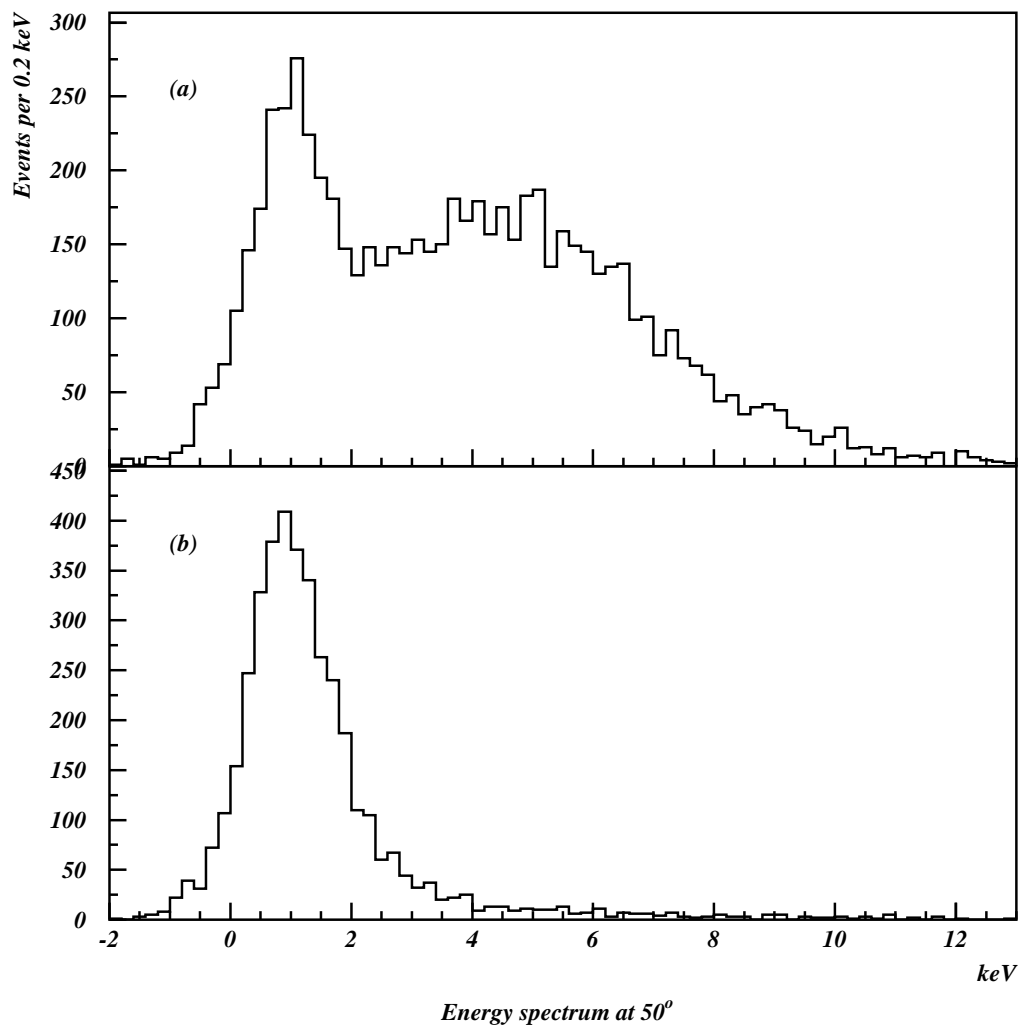


Figure 3: The energy spectra at 50° scattering angle for (a) events with high TOF values, (b) events with low TOF values.

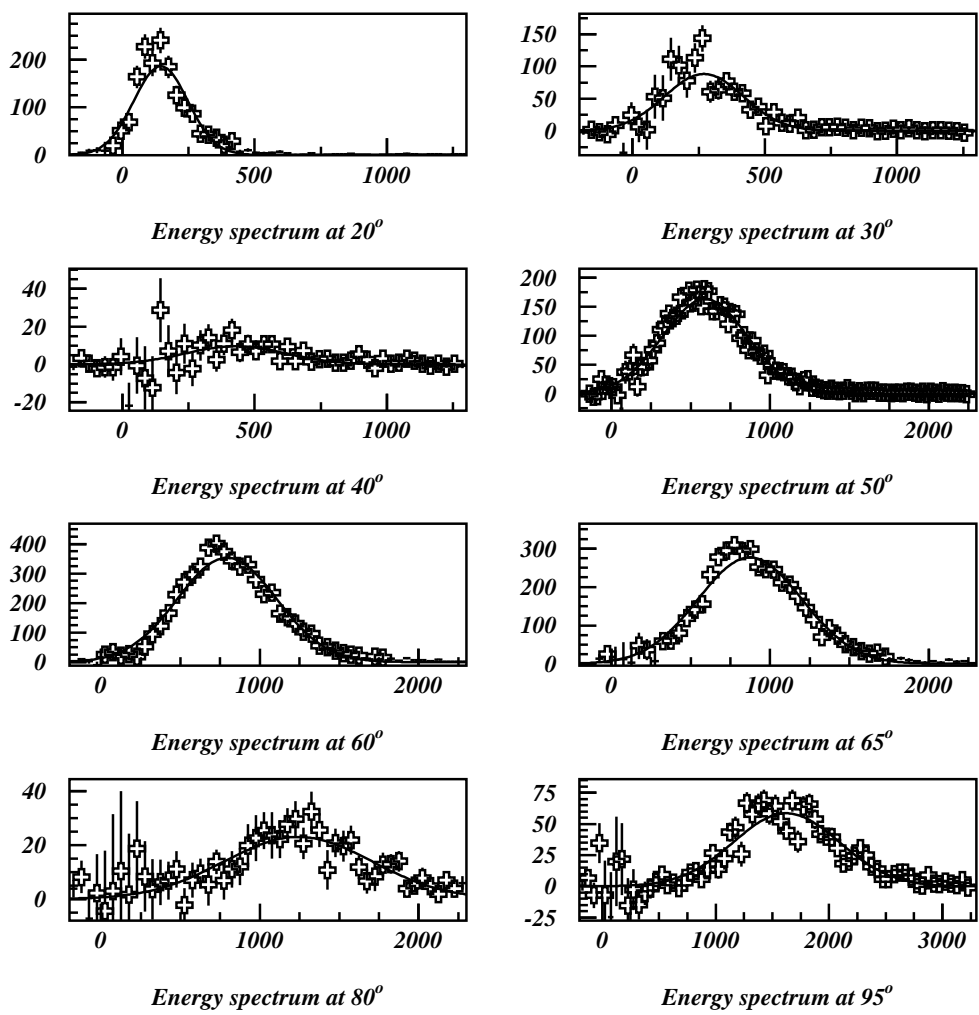


Figure 4: The observed energy spectra with background subtracted at different scattering angles.

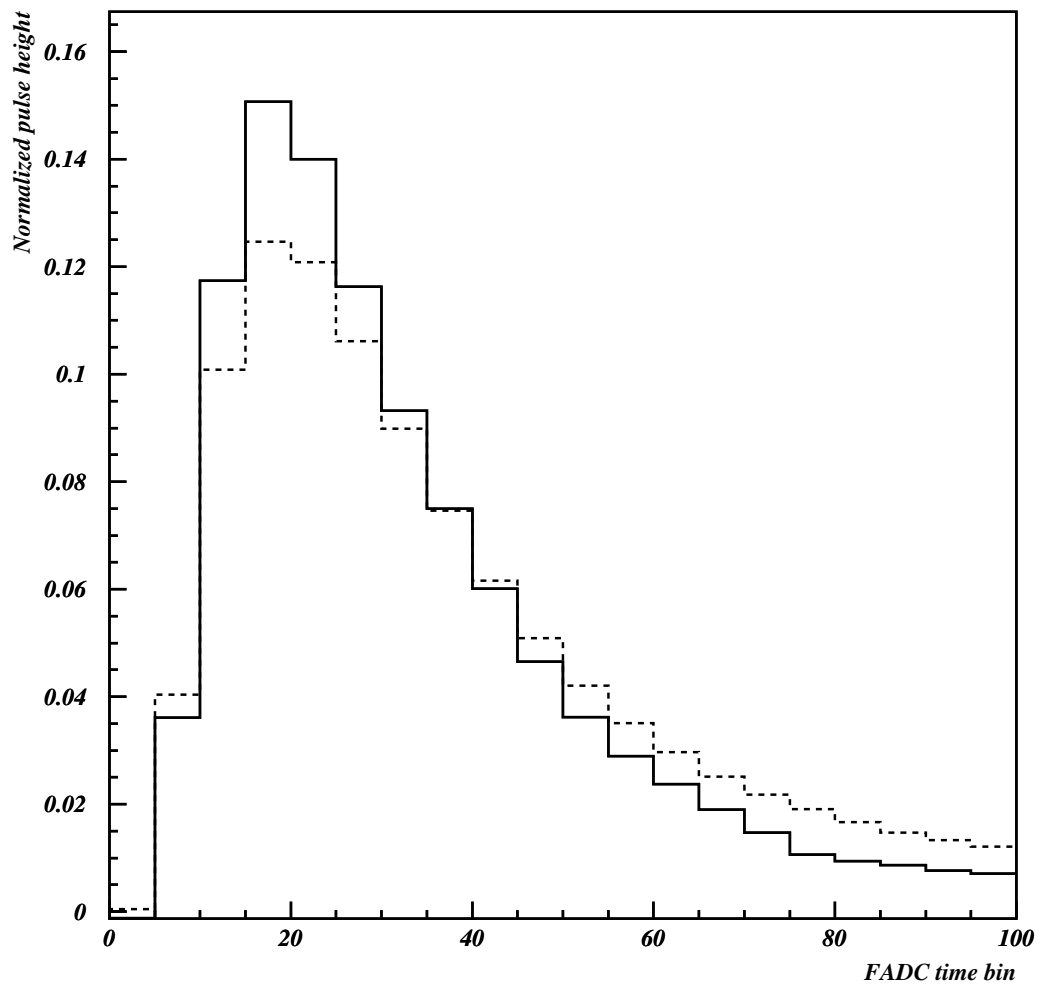
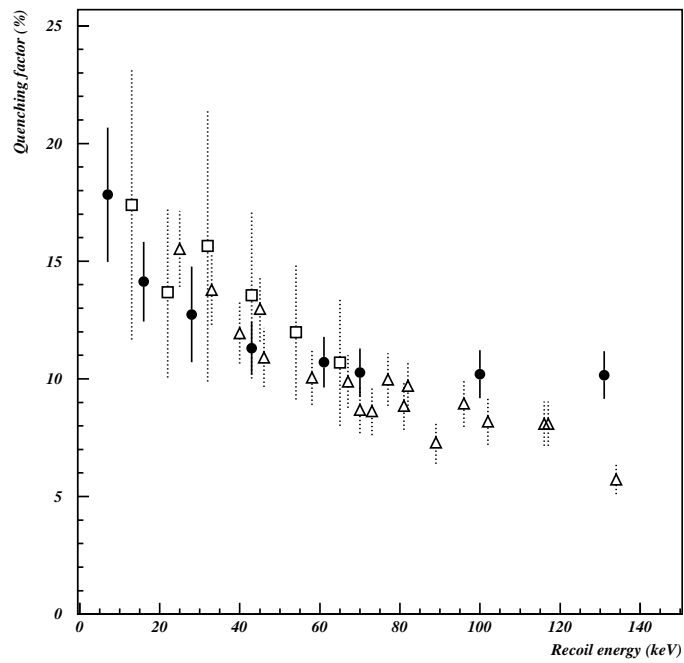


Figure 5: The normalized pulse shape in the first 100 FADC samplings at 50 ns per bin. Solid histogram is neutron data at 50° and dashed histogram is 22.1 keV X-ray data.

(a)



(b)

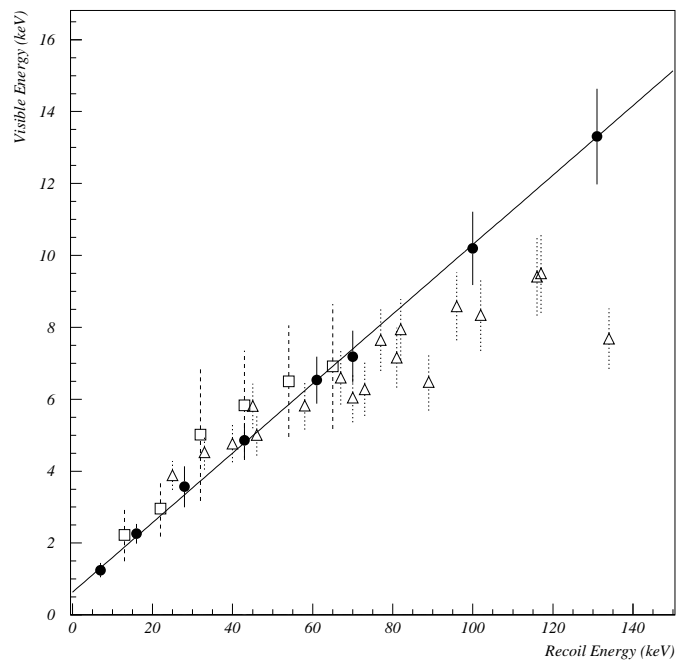


Figure 6: (a) The quenching factors and (b) electron-equivalence light yield versus recoil energy measured in this work shown as black circles. The solid line is a linear fit to the data. Open triangles and open squares are data from Ref. [8] and Ref. [9], respectively.

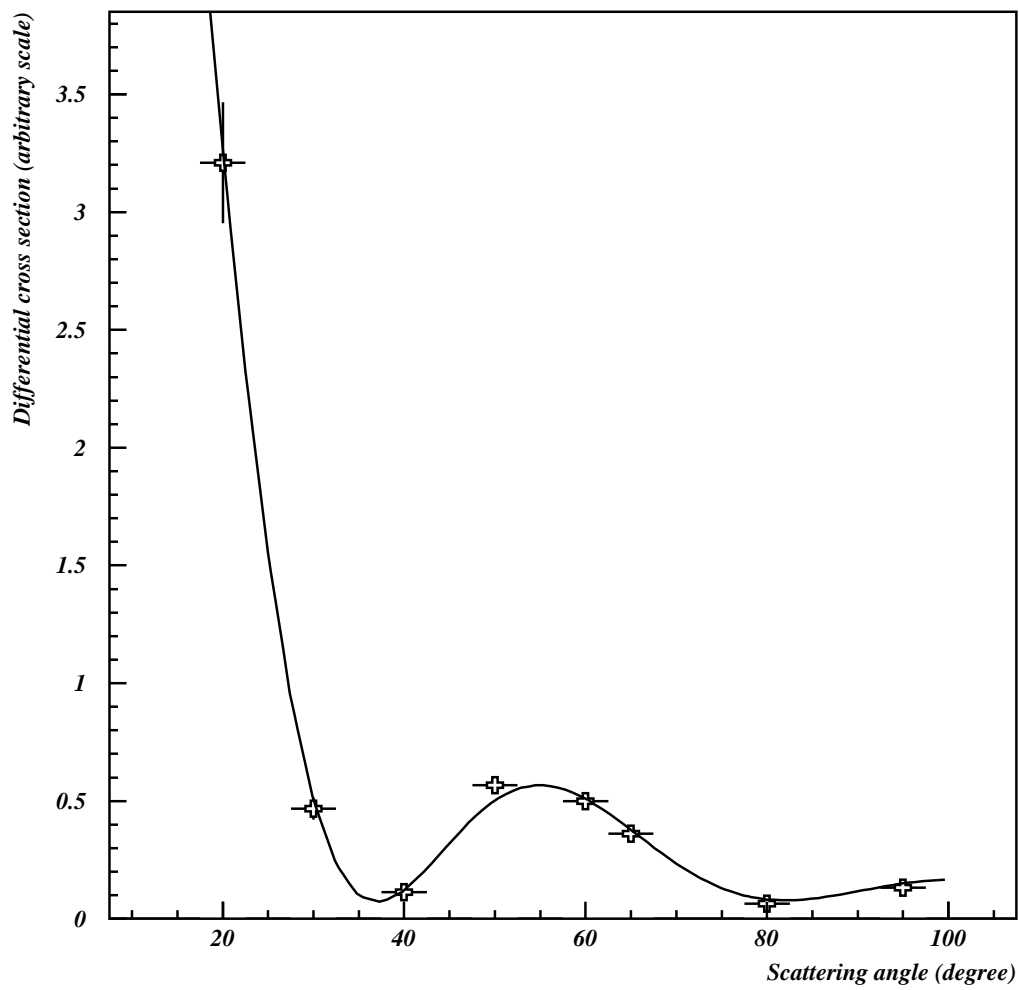


Figure 7: The differential cross sections determined from nuclear recoils in the target.

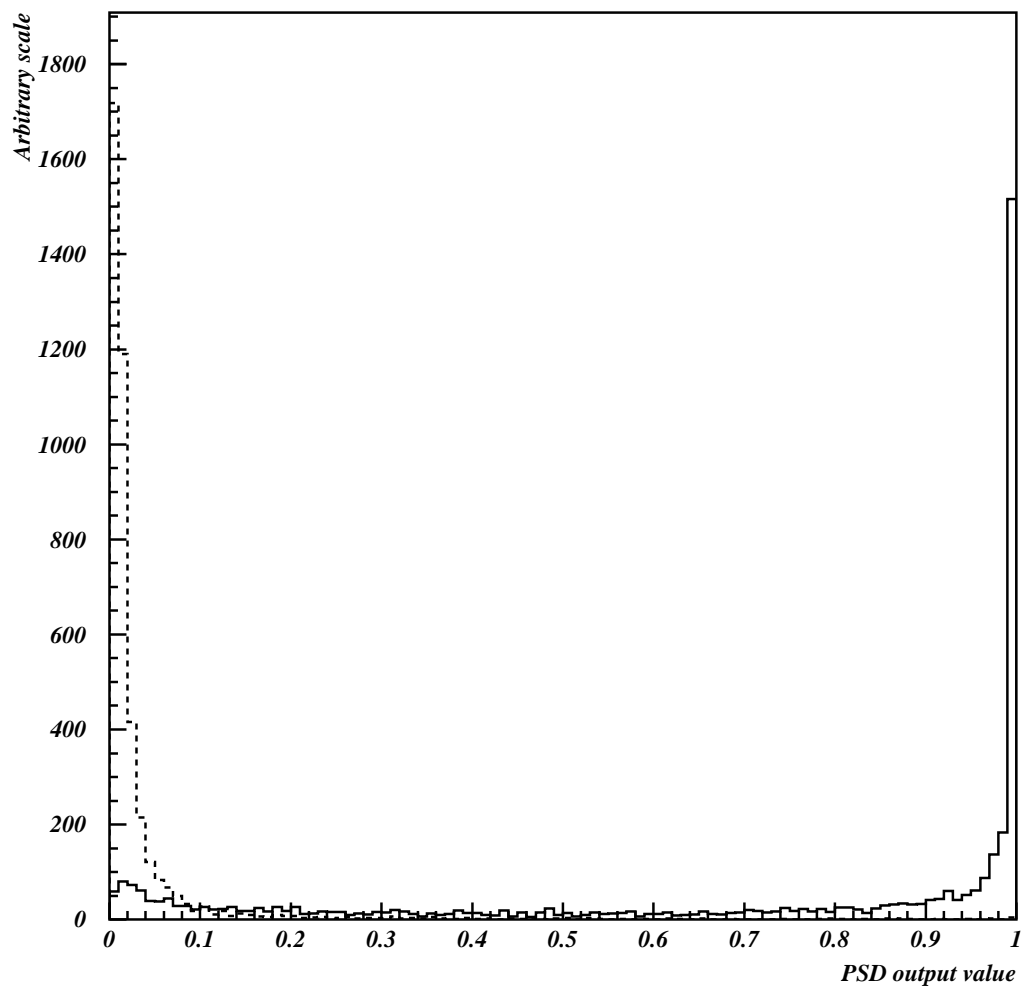


Figure 8: The neural network output of 4000 nuclear recoil events (solid histogram) and 4000 γ events (dashed histogram). The nuclear recoil energy is 43 keV and the γ energy is 22 keV.

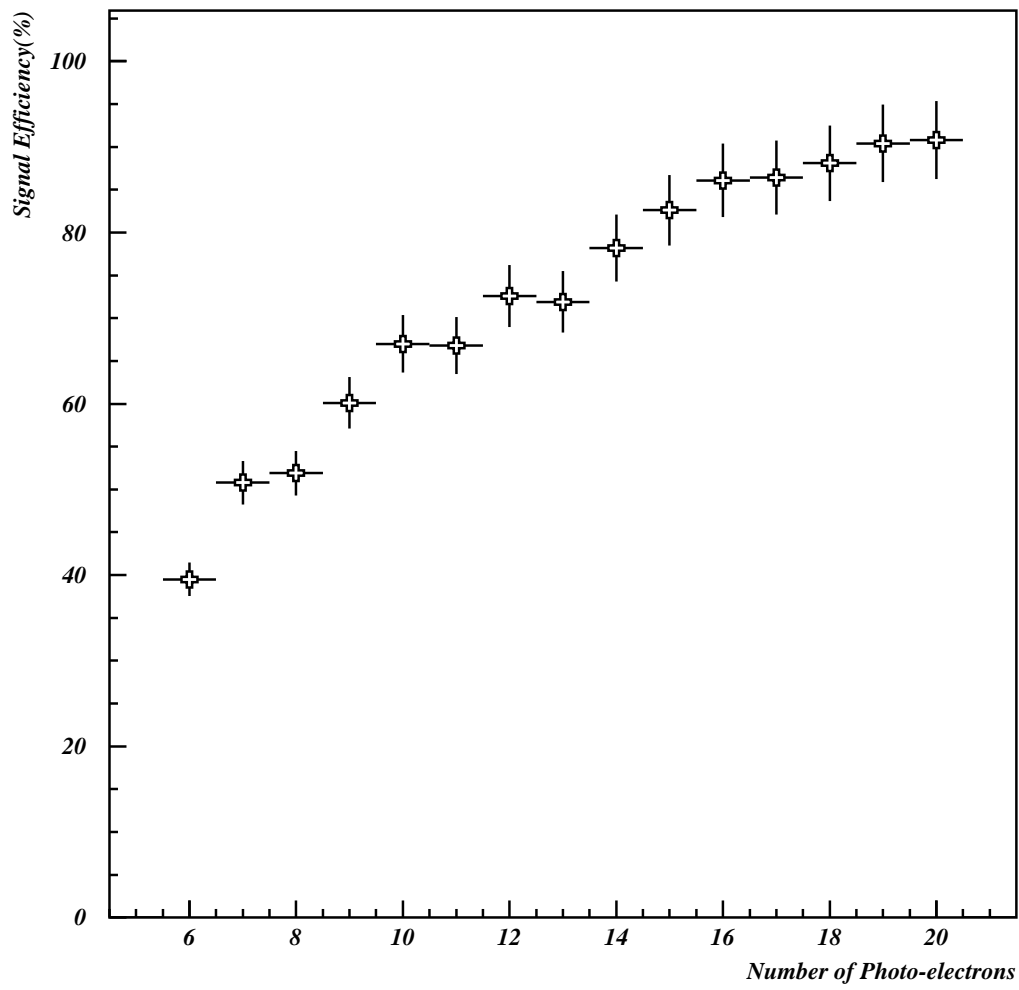


Figure 9: The PSD performance based on neural net studies. The γ rejection is fixed at 95% and the result of signal efficiency is plotted against available number of photo-electrons.

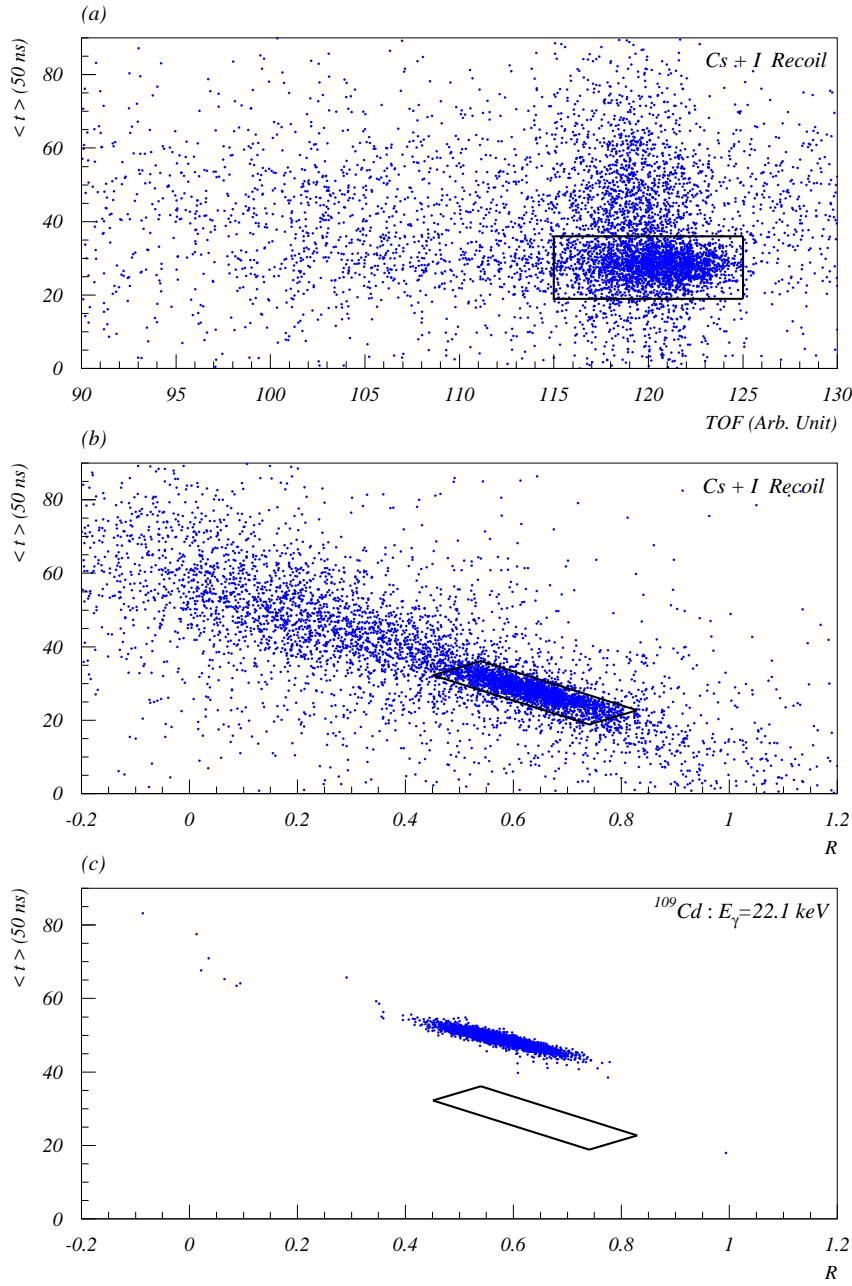


Figure 10: Scattered plots for the $\langle t \rangle$ parameter versus the (a) TOF values and (b) R parameters for the nuclear recoil events at 95° , and (c) for events due to the 22 keV γ -rays from a ^{109}Cd source. The box region represents the CsI nuclear recoil events, indicating clear separations from the accidental and “in-time” γ -background.

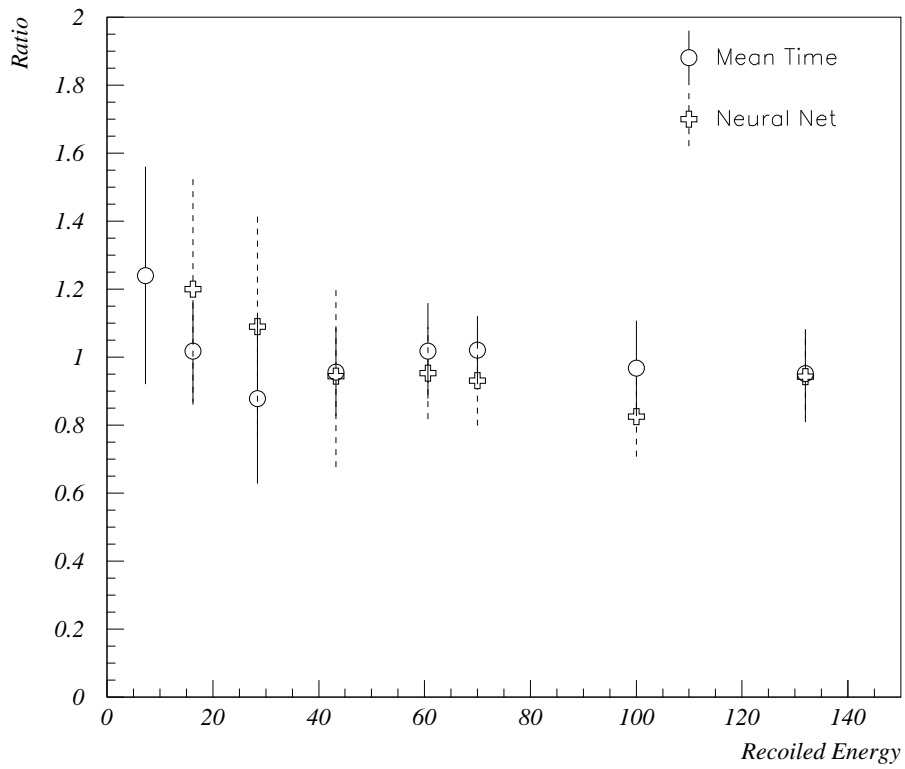


Figure 11: Ratio of electron-equivalence light yield derived from the two PSD algorithms, labelled “Mean Time” and “Neural Net”, with the measurements of the statistical subtraction method. Consistent results are obtained among them.

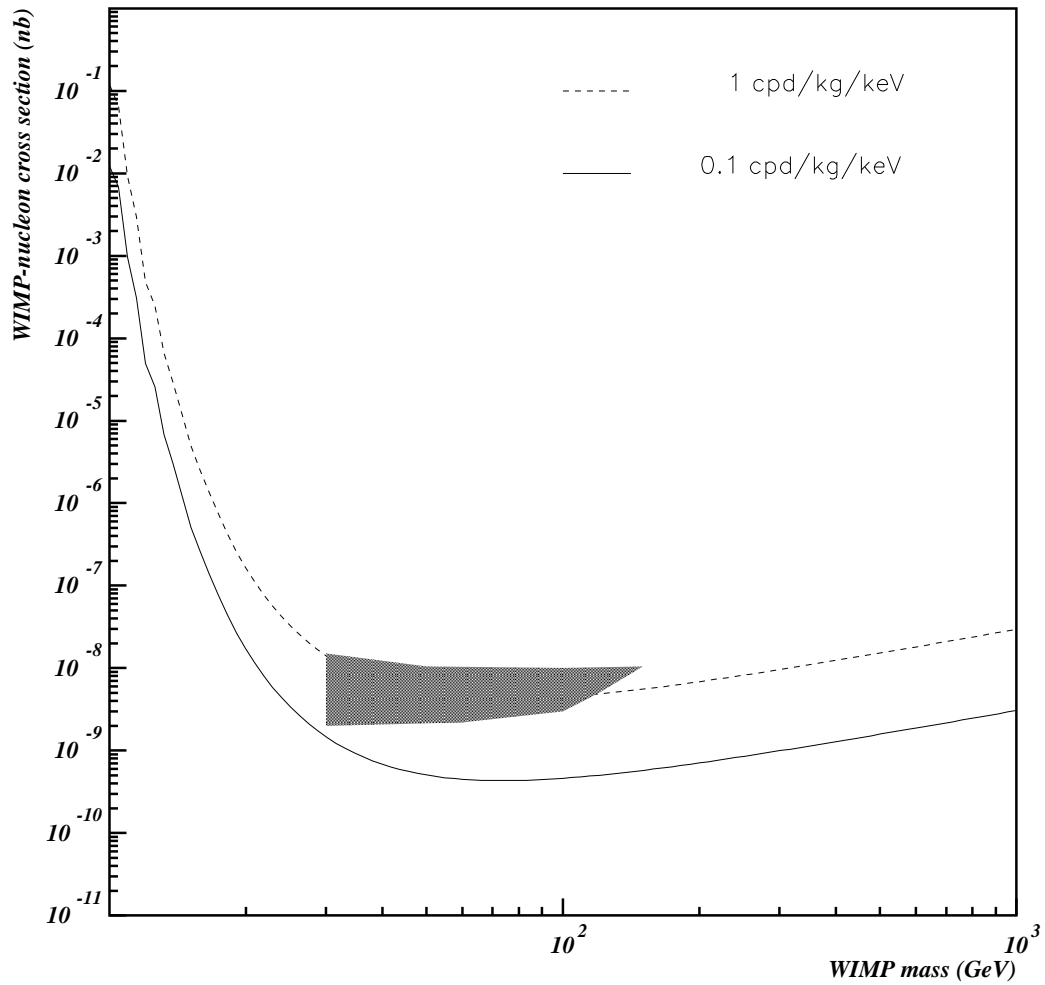


Figure 12: The sensitivity plot of cross-section versus WIMP mass on a 1 ton CsI(Tl) detector, with the assumptions that the detector threshold is set at 2 keV with a quenching factor of 0.13. The two cases of background counting rate at 1 and 0.1 counts per day (cpd) per kg per keV are shown. The DAMA allowed region is presented by the shaded area.